Elsevier Editorial System(tm) for Journal of Alloys and Compounds

Manuscript Draft

Manuscript Number:

Title: Yb3+:(LuxY1-x)2O3 mixed sesquioxide ceramics for laser applications. Part I: Fabrication, microstructure and spectroscopy

Article Type: Full Length Article

Keywords: (Yb:Lu,Y)2O3; Transparent ceramics; Microstructure; Raman spectroscopy, Lasers; Nanoparticles.

Corresponding Author: Dr. Guido Toci, Ph.D.

Corresponding Author's Institution: National Research Council, National Institute of Optics

First Author: Angela Pirri, Ph.D.

Order of Authors: Angela Pirri, Ph.D.; Guido Toci, Ph.D.; Barbara Patrizi; Roman N Maksimov, M.Sc.; Vladimir V Osipov, Prof.; Vladislav A Shitov; Artem S Yurovskikh; Egor V Tikhonov; Maurizio Becucci, Prof.; Matteo Vannini, Dr.

Abstract: We report an in-depth investigation (fabrication, microstructure and spectroscopy) of Yb3+-doped mixed sesquioxide transparent ceramics (LuxY1-x)2O3 with x = 0.0.113 and 0.232. The ceramics were fabricated by vacuum sintering of nano-sized particles synthesized by CO2 laser co-evaporation of the corresponding solid targets with different Y/Lu balance. The effect of Lu3+ concentration on crystal structure and phase evolution of the nanopowders and microstructure, optical and spectroscopic properties of the sintered ceramics was investigated. The micro-Raman measurements with high spatial resolution revealed a homogeneous distribution of both yttrium and lutetium in the mixed composition. The optical transmission of 1.4 mm-thick ceramics was over 80% in the wavelength range of 500-1100 nm. Partial substitution of Y3+ cations for Lu3+ cations determines a small shift toward longer wavelengths and broadening of the main emission peaks at about 1030 and 1076 nm. This is the first extensive characterization of the spectroscopic properties of Yb:(Y,Lu)2O3 compositional family in ceramic hosts.

Dear Editor,

please find enclosed the manuscript entitled

"**Yb^{3+} doped $(Lu_xY_{1-x})_2O_3$ mixed sesquioxide ceramics for laser applications. Part I: Fabrication method, microstructure analysis and spectroscopy characterization"**, by Angela Pirri, Guido Toci, Barbara Patrizi, Roman N. Maksimov, Vladimir V. Osipov, Vladislav A. Shitov, Artem S. Yurovskikh, Egor V. Tikhonov, Maurizio Becucci, Matteo Vannini (Corresponding Author: Guido Toci)

to be considered for publication in Journal of Alloys and Compounds.

The paper is linked to a second manuscript that we have just submitted for publication in the same Journal, namely

"Yb^{3+} doped $(Lu_xY_{1-x})_2O_3$ mixed sesquioxide ceramics for laser applications. Part II: Laser performances", by Guido Toci, Angela Pirri, Barbara Patrizi, Roman N. Maksimov, Vladimir V. Osipov, V.ladislav A. Shitov, Matteo Vannini (Corresponding Author: Angela Pirri)

The two papers deal with the extensive characterization of a set of transparent ceramic samples with composition (Lu,Y)2O3 and Yb doping for laser applications.

The Part I addresses, as indicated in the title, the preparation procedure, the microstructural and the spectroscopic characterization of the samples

The Part II is devoted to the comparative analysis of the laser emission performances of the same sample set

We decided to submit two separate manuscripts as the results of the investigation were too broad to be resumed in a single paper, but the two parts are strictly interconnected from the scientific point of view. Therefore, the two papers should be considered as a single, organic body of work in terms of their scientific evaluation, and (if accepted) they should be published simultaneously.

Please do not hesitate to contact us if you need any further information

Sincerely yours

The Authors

Prime Novelty Statement

We report for the first time an in-depth investigation (fabrication, microstructure and spectroscopy) of ceramic sesquioxide compositional family $(Lu_xY_{1-x})_2O_3$ with x = 0.0.113 and 0.232 and Yb doping for laser applications. The ceramics were fabricated by vacuum sintering of nano-sized particles synthesized by CO_2 laser co-evaporation of the corresponding solid targets with different Y/Lu balance. The effect of Lu^{3+} concentration on crystal structure and phase evolution of the nanopowders and microstructure, optical and spectroscopic properties of the sintered ceramics was investigated. The micro-Raman measurements with high spatial resolution revealed a homogeneous distribution of both yttrium and lutetium in the mixed composition. The optical transmission of 1.4 mm-thick ceramics was over 80% in the wavelength range of 500–1100 nm. The impact of the variation of the Lu/Y balance in the spectroscopic properties of the lasing dopant Yb^{3+} was analyzed.

The use of laser ablated nanoparticles allowed to obtain high optical quality ceramics directly from the sintering step, without the need of further steps (i.e. Hot Isostatic Press) to improve densification.

Partial substitution of Y^{3+} cations for Lu^{3+} determines a small shift toward longer wavelengths and broadening of the main emission peaks at about 1030 and 1076 nm. The overall structure of absorption and emission spectra is intermediate between those of $Yb:Lu_2O_3$ and $Yb:Y_2O_3$.

To the best of our knowledge, this is the first extensive characterization of the spectroscopic properties of $Yb:(Y,Lu)_2O_3$ compositional family, either in crystals and in ceramic hosts.

Yb^{3+}:$(Lu_xY_{1-x})_2O_3$ mixed sesquioxide ceramics for laser applications. Part I: Fabrication, microstructure and spectroscopy

Angela Pirri[a], Guido Toci[b,*], Barbara Patrizi[a], Roman N. Maksimov[c,d], Vladimir V. Osipov[c], Vladislav A. Shitov[c], Artem S. Yurovskikh[d], Egor V. Tikhonov[c], Maurizio Becucci[e], Matteo Vannini[b]

[a]Istituto di Fisica Applicata "N. Carrara", IFAC, Consiglio Nazionale delle Ricerche, CNR, Via Madonna del Piano 10C, I-50019 Sesto Fiorentino (FI) Italy
[b]Istituto Nazionale di Ottica, INO, Consiglio Nazionale delle Ricerche, CNR, Via Madonna del Piano 10, I-50019 Sesto Fiorentino (FI) Italy
[c]Institute of Electrophysics UrB RAS, Amundsen St. 106, Ekaterinburg 620016, Russia
[d]Ural Federal University named after the first President of Russia B.N. Yeltsin, Mira St. 19, Ekaterinburg 620002, Russia
[e]Dipartimento di Chimica "U. Schiff", Università di Firenze, Via della Lastruccia, 3-13, I-50019 Sesto Fiorentino (FI), Italy

*Corresponding Author: Tel. +39 (0)55 5225315; e-mail: guido.toci@ino.cnr.it

Abstract

We report an in-depth investigation (fabrication, microstructure and spectroscopy) of Yb^{3+}-doped mixed sesquioxide transparent ceramics $(Lu_xY_{1-x})_2O_3$ with x = 0.0.113 and 0.232. The ceramics were fabricated by vacuum sintering of nano-sized particles synthesized by CO_2 laser co-evaporation of the corresponding solid targets with different Y/Lu balance. The effect of Lu^{3+} concentration on crystal structure and phase evolution of the nanopowders and microstructure, optical and spectroscopic properties of the sintered ceramics was investigated. The micro-Raman measurements with high spatial resolution revealed a homogeneous distribution of both yttrium and lutetium in the mixed composition. The optical transmission of 1.4 mm-thick ceramics was over 80% in the wavelength range of 500–1100 nm. Partial substitution of Y^{3+} cations for Lu^{3+} cations determines a small shift toward longer wavelengths and broadening of the main emission peaks at about 1030 and 1076 nm. This is the first extensive characterization of the spectroscopic properties of Yb:$(Y,Lu)_2O_3$ compositional family in ceramic hosts.

Keywords: $(Yb:Lu,Y)_2O_3$; Transparent ceramics; Microstructure; Raman spectroscopy, Lasers; Nanoparticles.

1. Introduction

In recent years, several efforts have been made to obtain laser materials with broad emission band for the generation and amplification of ultrashort laser pulses. Yb^{3+} ion as a lasing dopant has several useful features that have determined its success in laser applications. Nonetheless, in the

majority of hosts Yb^{3+} has a relatively narrow emission bandwidth, in comparison for instance with Ti:Sapphire, which makes it difficult the generation [[1]] and in particular the amplification [[2]] of laser pulses below 100 fs of duration.

To overcome this difficulty, many studies addressed the so-called mixed hosts, *i.e.* solid solutions of chemically compatible materials, where the disordered lattice structure resulting from the solid solution can induce an inhomogeneous broadening of the absorption and emission spectra. Several Yb^{3+}-doped compositions, both ceramics [[3]-[6]] and crystals [[7]-[10]] have been tested. An analysis of crystalline Yb doped mixed sesquioxides was reported by Beil *et al.* [[11]] where a significant broadening in the emission spectrum was found in particular for Yb:$(Lu,Sc)_2O_3$ matrices.

Lattice disorder and inhomogeneous broadening can also be induced by the incorporation of further co-dopants. This has been suggested by Bagayev *et al.* [[12]], which reported the fabrication and preliminary laser emission results of ceramics with composition $(Yb_{0.01}Lu_{0.24}Y_{0.75})_2O_3$. ZrO_2 was included as sintering aid to avoid exaggerated grain growth and formation of intragranular pores but it could also contribute to the overall lattice disorder of the host matrix (due to the large ionic radius mismatch and the excess charge (Zr^{4+}) with respect to the substituted ion (Y^{3+} or Lu^{3+}). Further, continuous-wave, mode-locked and Q-switched laser operation was demonstrated using Tm^{3+}-doped $LuYO_3$ mixed sesquioxide ceramics [[13],[14]] but details on the raw powders, fabrication method and microstructure properties of the obtained samples were not discussed.

High purity ultrafine powders are very important for the preparation of laser-grade ceramics. As for the disordered compositions, the desired sesquioxides should be homogeneously mixed together on a low scale to avoid refractive index modulation around grain boundaries caused by point-to-point variation in the lattice structure. Laser ablation method is well suited to the synthesis of loosely agglomerated nano-sized powders with narrow particle size distribution. In addition, the required sesquioxides can be mixed on atomic scale at high temperature to achieve uniform distribution of chemical species in the volume of individual nanoparticles.

This work extends our previous study [[15]] on the fabrication, the structural and the spectroscopic characterization of a series of Yb^{3+}-doped mixed sesquioxide transparent ceramics $(Lu_xY_{1-x})_2O_3$ (x =0; 0.113 and 0.232) based on laser ablated nanopowders. These compositions were selected because Y_2O_3 matrix is one of the most attractive ceramic hosts [[16]-[18]]; it has a high thermal conductivity (literature data span from 13.6 W/m K [[19]] to ~17 W/m K [[20]]), a sustainable sintering temperature (~1700°C), a low effective phonon energy [[19]], which reduces the probabilities for non-radiative transitions. A reasonable level of disorder in the hosts is expected due to the presence of Lu^{3+} and Zr^{4+} ions as well, leading to a broadening the absorption and emission bandwidths.

The ceramic samples, fabricated by using solid-state sintering of mixed sesquioxide nanoparticles under vacuum, were carefully tested. In particular, the microstructure of the samples was analyzed by means of X-ray diffraction to determine the lattice constants, and electron microscopy to assess the morphology and grain structure. Micro-Raman spectroscopy was used to evaluate the composition uniformity at the sub-grain size scale. Spectroscopic characterization included absorption and emission spectra at room temperature.

2. Materials and experimental details

2.1. Synthesis of mixed sesquioxide nano-sized particles

Commercially available high-purity powders of Yb_2O_3, Lu_2O_3 and Y_2O_3 (>99.95% TREO, Lanhit Company, Russia) were used as raw materials for the preparation of laser media. These sesquioxides powders were dry-mixed together for 24 h in a rotary mixer with an inclined axis of rotation to form $(Yb_{0.05}Lu_xY_{1-x})_2O_3$ powder blends where x = 0; 0.15 and 0.25. Around 2 wt.% of zirconium dioxide was added to each composition as a sintering additive. The obtained blends were then compacted into cylindrical-shaped green targets with a diameter of ~66 mm by uniaxial static pressing at 10 MPa and pre-sintered at 1100 °C for 5.5 h in air. After pre-sintering the relative density of laser targets reached 55% with respect to the theoretical density.

The obtained powder targets were ablated in air flow of atmospheric pressure using a pulse-periodical carbon dioxide laser “LAERT” [[21],[22]]. The main experimental parameters were as follows: pulse energy – 0.9 J, pulse duration – 330 μs, pulse repetition rate – 500 Hz, peak power – 7 kW, average power – 450 W. The laser beam was focused into 0.75 mm × 0.9 mm-sized elliptical spot by a KCl lens with a power density of 1.3 MW/cm^2. The linear velocity of laser beam movement was 35 cm/s. The production rate of nanopowders was from 15 to 25 g/h depending on the composition of laser target.

The phase evolution of the nanopowders was studied during heating up to 1100 °C in air by means of non-ambient X-Ray diffraction using D8 Advance diffractometer (Bruker AXS, Germany) with Anton-Paar HTK 1200N high temperature chamber in the 25°…35° 2θ range in Cu Kα radiation. The morphology of the obtained nanopowders was observed using a JEOL JEM 2100 (JEOL Ltd., Japan) transmission electron microscope (TEM). The chemical composition of the as-synthesized nanopowders was analyzed using an Optima 2100 DV inductively coupled plasma mass spectrometer (ICP MS, Perkin Elmer, USA).

2.2. Fabrication of transparent Yb:(Lu,Y)$_2$O$_3$ ceramics

The ceramic samples were fabricated using solid-state vacuum sintering of mixed sesquioxide nanoparticles. Annealed nano-sized particles with the proper Y/Lu balance and cubic crystal

structure were uniaxially dry-pressed at 200 MPa into a 15-mm-diameter cylindrical pellets. After removing the organic components by calcining (800 °C, 3 h), the green compacts were sintered at 1780 °C for 20 h under 10^{-3} Pa vacuum. The sintered ceramic samples were then annealed (1400 °C, 2 h) to eliminate the oxygen vacancies and mirror polished on both sides. Fig. 1 shows the picture of the three samples used in the experiments.

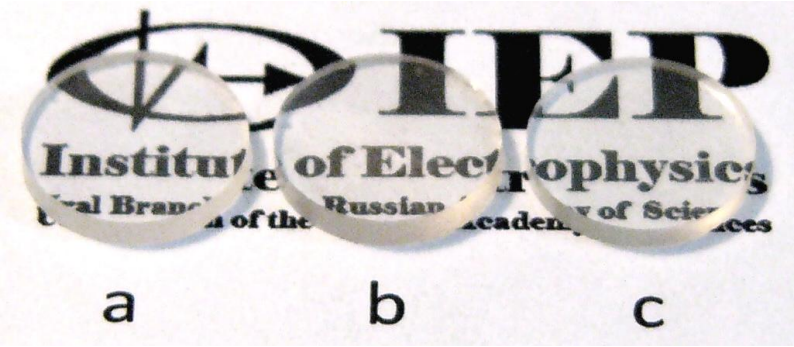

Fig. 1. Photograph of the fabricated and polished ceramic samples: (a) – $(Yb_{0.056}Y_{0.944})_2O_3$; (b) – $(Yb_{0.056}Lu_{0.113}Y_{0.831})_2O_3$; (c) – $(Yb_{0.059}Lu_{0.232}Y_{0.709})_2O_3$.

The microstructure of the polished and thermally etched surface of the sintered samples was analyzed using a scanning electron microscope AURIGA CrossBeam (SEM, Carl Zeiss NTS, Germany). The average grain size of the obtained transparent ceramics was determined by the linear intercept method from SEM images using a three dimensional correction factor of 1.571. The phase composition of the ceramics was examined by an X-ray diffractometer Bruker D8 Advance (Bruker AXS, Germany) using Cu Kα radiation.

2.3. Optical and spectroscopic characterization

The internal homogeneity of the samples, on a spatial scale smaller than the grain size, was studied by means of micro-Raman spectroscopy. This technique provides complementary information with respect, for instance, to XRD and Energy Dispersive X-Ray Analysis, EDX, especially to enlighten the possible presence of segregation effects between Lu^{3+} and Y^{3+} ions. Micro-Raman spectroscopy provides a higher spatial resolution with respect to XRD (down to 1 μm scale, whereas transverse spatial resolution of XRD is usually of the order of 1 mm, and the probed volume involves the whole sample thickness); with respect to EDX, it provides information about the chemical structure and not only on the elemental composition, thus being, at least in principle, capable to discriminate between different crystalline phases. Finally, in optically transparent materials it can be used to probe in depth the volume of the sample and not only its surface.

The samples were analyzed by means of a micro-Raman spectrometer RM2000 (Renishaw, Wotton-under-Edge, UK) equipped with a 50x/0.80N.A Olympus microscope objective and a laser-diode excitation-source at 785 nm. The microscope is equipped with motorized slits, computer

controlled to a spatial accuracy better than 1 μm. The spectral calibration of the spectrometer was checked on the 520 cm^{-1} first order Raman band of bulk silicon; the spectral resolution was 7 cm^{-1} (equivalent to 3 pixels on the CCD camera) as verified from linewidth measurements on the same silicon calibration band [[23]].

For this analysis, samples of 3*at.%* Yb:Y_2O_3 ceramics (also prepared at the Institute of Electrophysics UrB RAS) and 1*at.%* Yb:Lu_2O_3 ceramics (from Konoshima Chemical Corp.) were included in the samples set, to have reference spectra for both the end compositions. No attempt was made to assign the Raman shift frequencies to specific lattice vibration modes, as this was beyond the purpose of this analysis. The spatial homogeneity of the samples was checked by acquiring Raman spectra in several points (usually 20) of each sample along a line, with fine (1 μm) and coarse (50 μm) spacing, at a depth of about 300 μm below the sample surface.

The transmission spectra of the samples were acquired by means of a Perkin Elmer Lambda 1050 spectrometer in the interval between 200 nm and 1100 nm with a spectral resolution of 1 nm.

The lifetime of the Yb^{3+} $^2F_{5/2}$ state was measured by the pinhole method to avoid radiation trapping effects, using the experimental set up and the data acquisition procedure similar to those already described in [[24],[25]]. Fluorescence spectra were acquired with a miniaturized spectrometer equipped with a 1630 channels CMOS linear array detector. To avoid reabsorption effects the samples were excited with a pulsed Ti:Sapphire laser at 896 nm, in a small spot, very near to a lateral edge of the sample; the fluorescence was collected at 90° with respect to the excitation beam.

3. Results and discussions

3.1. Characteristics of Yb:(Lu,Y)$_2O_3$ nanopowders

To determine the exact Yb doping concentration and Y/Lu balance, we analyzed the chemical composition of the obtained nanopowders using ICP MS. The designed and final compositions are listed in Table 1. It appears that the evaporation rate is in the following descending order: Yb_2O_3 > Y_2O_3 > Lu_2O_3. The vapour stream of most refractory material (Lu_2O_3) is smaller than that of easily melted component so the melt in laser crater is depleted with the latter. The melt is squeezed out of the crater as an external rim or sprayed in the form of droplets and then the laser radiation again evaporates the material of powder target, which is not depleted with the easily melted sesquioxide, leading to enrichment of the mixed compositions by Yb_2O_3 and Y_2O_3. Laser power density is the most essential parameter affecting the alteration of chemical composition of the obtained nanopowders with respect to the composition of initial laser target.

Table 1. Designed and resultant chemical compositions of Yb:$(Lu,Y)_2O_3$ nanopowders. Also reported is the measurement error.

Composition of laser target			Composition of nanopowder		
Yb_2O_3, mol.%	Lu_2O_3, mol%	Y_2O_3, mol.%	Yb_2O_3, mol.%	Lu_2O_3, mol%	Y_2O_3, mol.%
5.0±0.5	0	95.0±0.5	5.6±0.6	0	94.4±0.6
5.0±0.5	15.0±1.5	80±2	5.6±0.6	11.3±1.1	83.1±1.7
5.0±0.5	25.0±2.5	70±3	5.9±0.6	23.2±2.3	70.9±2.9

For sake of clarity, from here on the samples $(Yb_{0.056}Lu_{0.113}Y_{0.831})_2O_3$ and $(Yb_{0.059}Lu_{0.232}Y_{0.709})_2O_3$ will be called Lu11 and Lu23 while the $(Yb_{0.056}Y_{0.944})_2O_3$ will be named Lu0.

Most of rare-earth sesquioxides evaporated by laser radiation condense into ultrafine spherical nanoparticles exhibiting a metastable monoclinic phase. It is suggested to perform the monoclinic to cubic phase conversion before compaction and sintering stages to prevent formation of core-shell structure and possible fracturing of ceramic sample due to an increase in the volume of unit cell. [[26]]. Fig. 2 shows the phase evolution of Lu11 powder during heating up to 1100 °C, monitored by means of XRD of the characteristic (222) diffraction peak. When the temperature is below 850 °C, there is no significant change in the collected patterns except the diffraction peaks shift to the lower angle values due to lattice expansion. The onset of the monoclinic to cubic phase transition at 850 °C is confirmed by an increase in intensity of the characteristic (222) line of the cubic phase at $2\theta \sim 29°$. As the temperature increases, the intensities of peaks corresponding to the monoclinic modification of Y_2O_3 decreases and both the monoclinic and cubic phases coexist up to about 1000 °C. Finally, heat treatment at 1050°C produced mixed sesquioxide nanoparticles exhibiting pure cubic phase, space group Ia3 as identified by ICDD PDF No. 00-067-0067. It appears that the temperature required for a complete phase transformation slightly decreases with the additions of Lu_2O_3 into Yb:Y_2O_3.

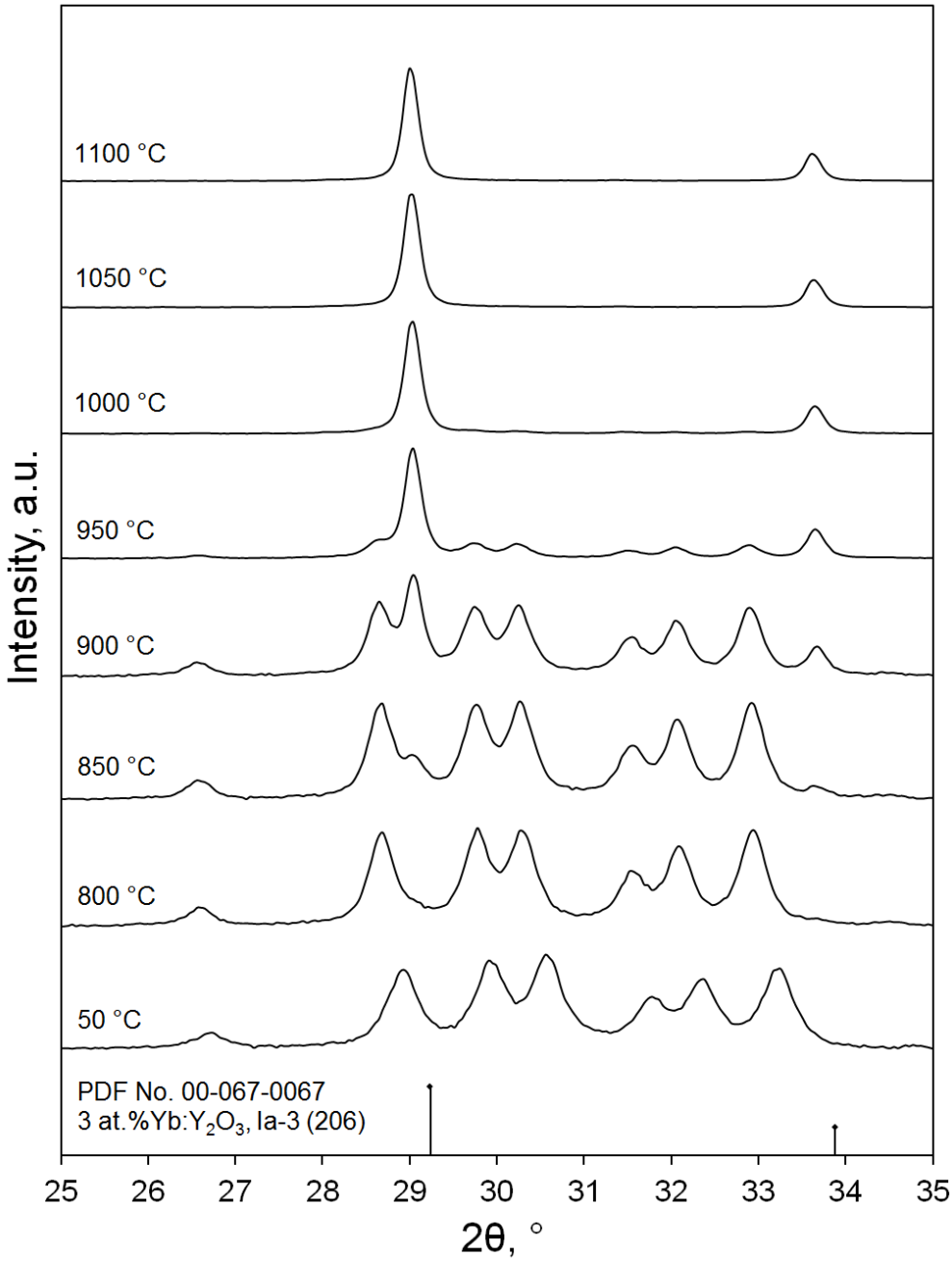

Fig. 2. Thermal X-ray analysis data showing the phase evolution of $(Yb_{0.056}Lu_{0.113}Y_{0.831})_2O_3$ nanopowder during heating up to 1100 °C in air.

The typical morphology of the obtained nanoparticles before and after calcination is shown in Fig. 3. The as-synthesized powder is in the form of soft aggregates consisting of nano-sized spherical shaped particles with an average size of ~20 nm. After calcination at 1050 °C for 1 h the sample showed interparticle neck growth along with the shape change from sphere to polyhedron. From BET analysis (TriStar 3000, Micromeritics, USA), we determined the specific surface areas of the as-synthesized and annealed powders as 41.9 m^2/g and 25.3 m^2/g, respectively so the

equivalent particle size increased from 23 nm to 39 nm, which is in good agreement with TEM observations.

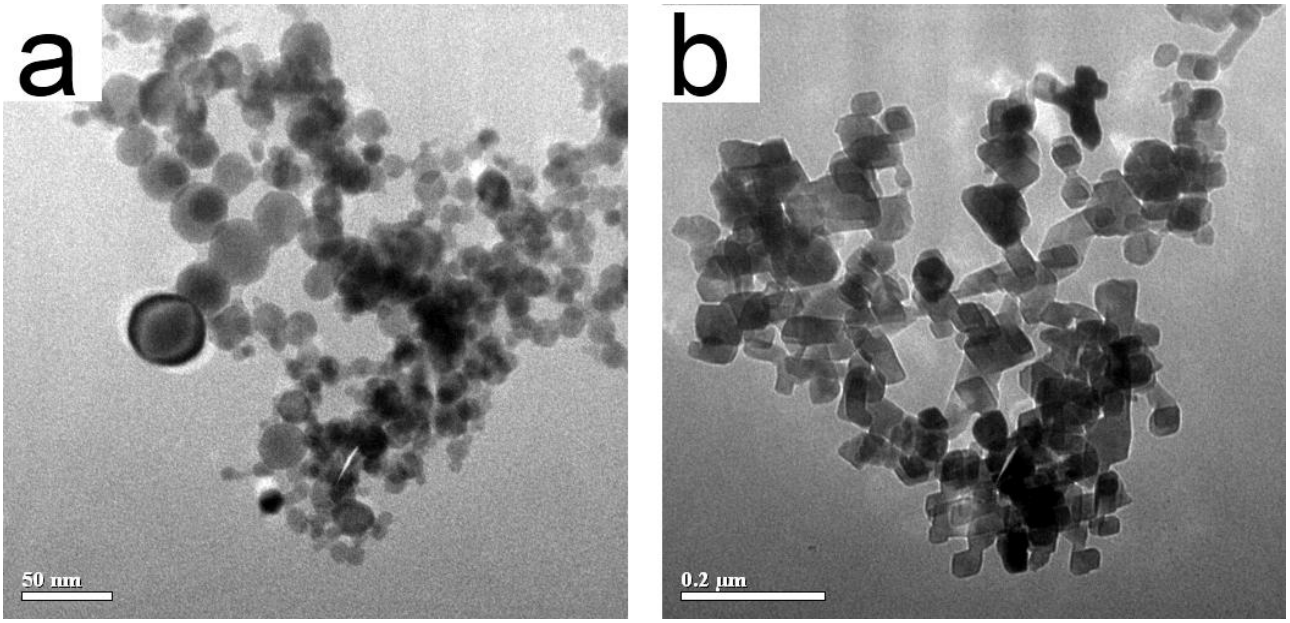

Fig. 3. TEM images showing the morphology of the as-synthesized (a) and annealed (b) $(Yb_{0.056}Lu_{0.113}Y_{0.831})_2O_3$ nanoparticles.

Compared with Yb-fiber laser emitting at the wavelength of 1.075 μm, the radiation of carbon dioxide laser (λ=10.6 μm) is more suitable for ablation of the Yb:$(Lu,Y)_2O_3$ targets. Rare-earth sesquioxides possess relatively large energy bandgap (~6-9 eV) and these materials are transparent for the radiation of Yb-fiber laser. The laser emission at λ=1.075 μm is absorbed by pores and structural defects and penetrates through the powder target to a depth of up to a few hundred microns. A propagating heat wave resulted in splintering of subsurface and highly irregular surface morphology leading to a significant decrease in the production rate of nanopowder. On the other hand, the laser emission at λ=10.6 μm penetrates to a depth of only several microns since the radiation is absorbed and scattered by optical phonons and phonon substructure, respectively. In this case, with respect to Yb-fiber laser, the greater part of lasing energy is spent for the evaporation of the material.

3.2. Microstructure analysis of transparent ceramics

A SEM micrograph showing the grain structure of Lu23 ceramics is presented in Fig. 4. The structure consists of tightly packed equiaxed crystallites with clean grain boundaries and no grain entrapped pores were detected. SEM observation of Lu0 and Lu11 samples did not demonstrate significant differences in morphology with respect to Lu23 ceramic shown in Fig. 4, so the corresponding images are not given here. The average grain size slightly increases with Lu

concentration, *i.e.* from 7.3 μm to 8.1 μm for Lu concentration from 0 to 23.2 mol.%. In other terms, higher Lu^{3+} concentration induces significant disordering of crystal lattice leading to the acceleration of diffusion processes and increase of grain size. Several spherical shaped pores with an average size of around 2 μm were observed throughout the depth of the samples using an optical microscope Olympus BX51TRF (Olympus Corp., Japan). We evaluated the content of the scattering centers in ceramics by direct count method as 1.3, 3.9 and 4.2 ppm for Lu0, Lu11 and Lu23 samples, respectively. Consequently, in our experimental conditions the substitution of up to ~23 at.% of Y for Lu in Yb:Y_2O_3 lattice barely influences the possible optical loss originated from the residual porosity. This statement will be additionally confirmed by the measurements of transmission spectra (see Section 3.3).

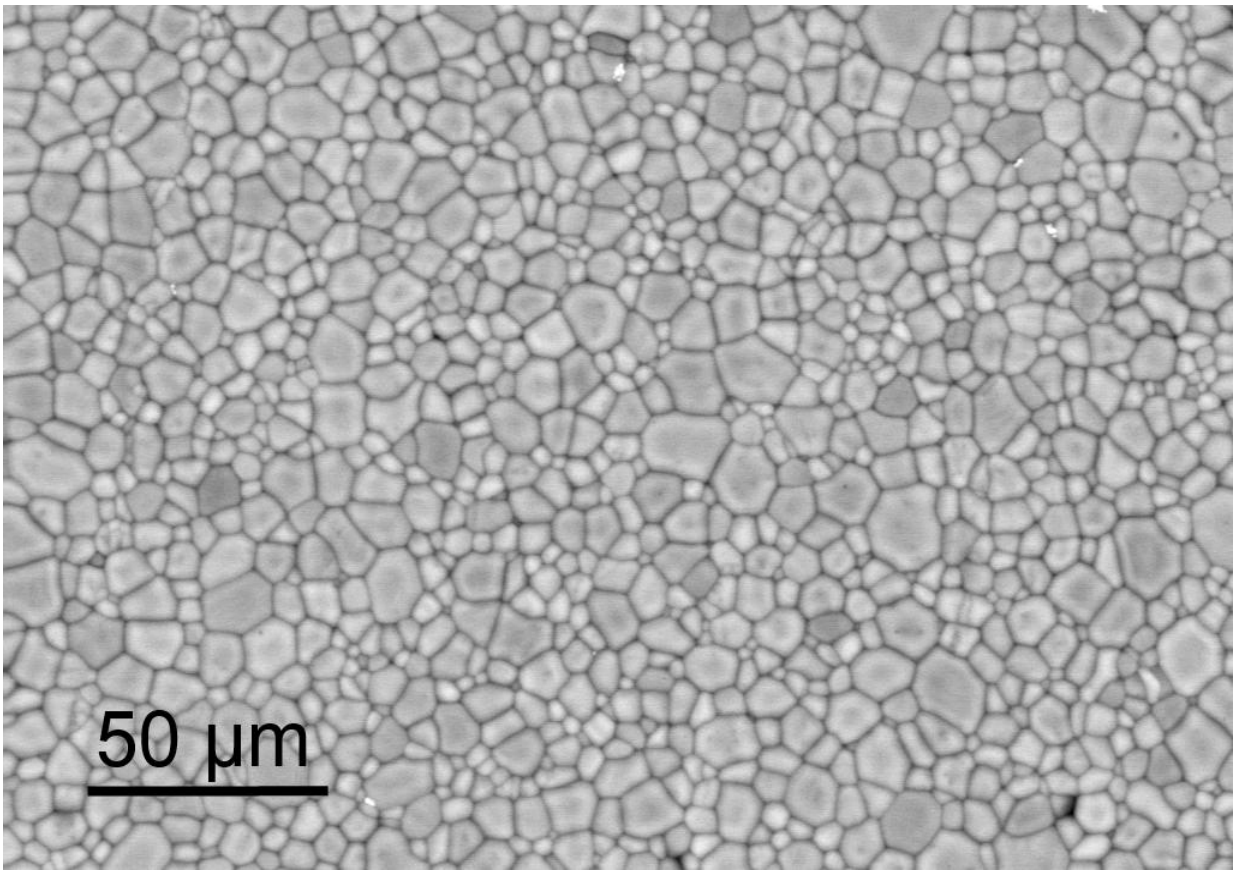

Fig. 4. SEM image of the thermally etched surface of the $(Yb_{0.059}Lu_{0.232}Y_{0.709})_2O_3$ ceramic sample showing its microstructure.

The X-Ray diffractograms for the sintered ceramics are shown in Fig. 5. The observed diffraction patterns for Lu0 sample can be well indexed to the solid solution of $(Yb_{0.056}Y_{0.944})_2O_3$ (space group Ia3-T_7^h) as identified by ICDD PDF No. 00-067-0067. Considering that both Y_2O_3 and Lu_2O_3 sesquioxides have the same cubic crystal structure, no other impurity phase was found in Lu11 and Lu23 ceramics. The diffraction peaks of secondary phases based on ZrO_2 were not observed taking into account the detection limit of about 3 wt.%. In addition, since the effective

ionic radius of Lu^{3+} (0.848 Å) is smaller than that of Y^{3+} (0.892 Å), the introducing of Lu^{3+} cations into Y_2O_3 matrix forms compressive strain and causes a certain degree of lattice disorder. Thus the diffraction peaks deflect toward larger angles with an increase in Lu_2O_3 content and the lattice constant decreases from 10.590 Å (Lu0 sample) to 10.561 Å and 10.538 Å for Lu11 and Lu23 doping concentrations. It must be noticed that the small splitting of the diffraction peaks in Fig. 5 is due to the use of the Cu Kα doublet as probe radiation (as the device is not equipped with monochromator), and not to the occurrence of separate lattice phases.

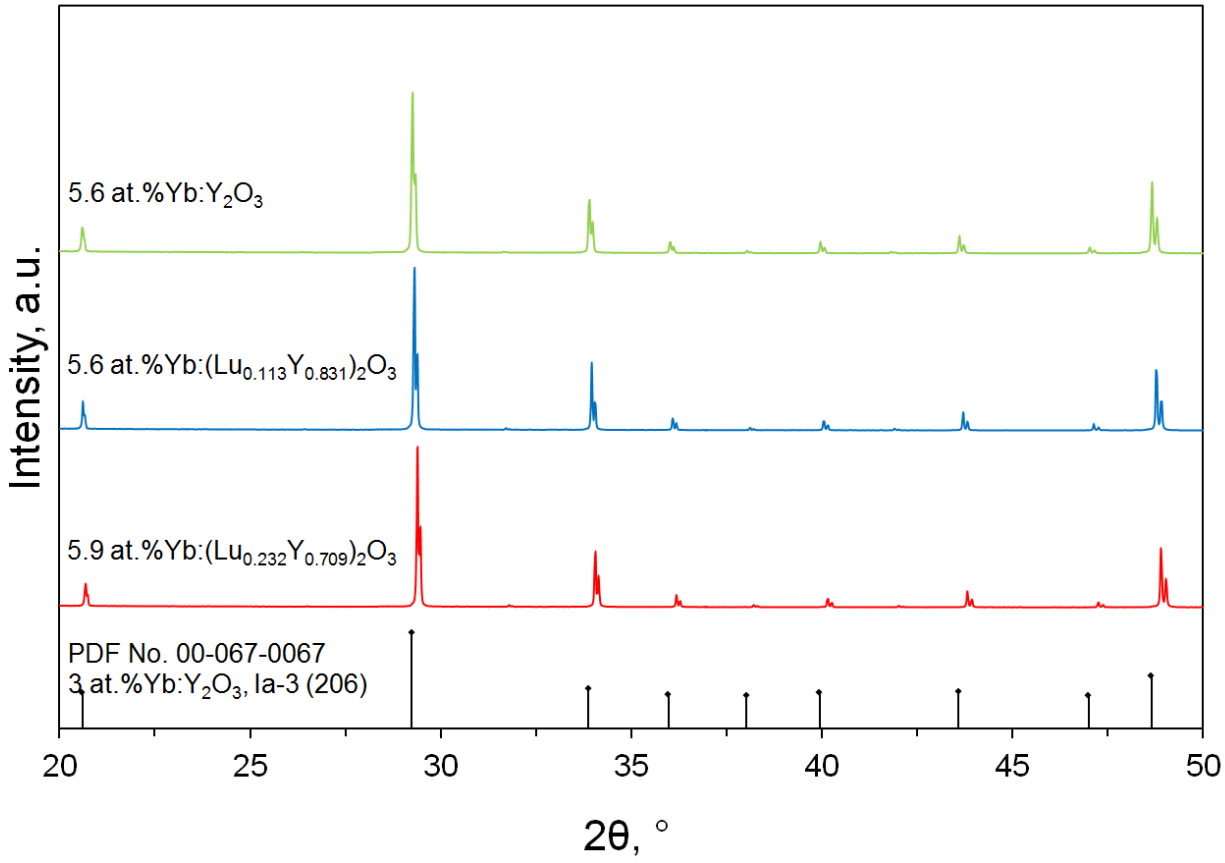

Fig. 5. X-ray diffraction patterns of the sintered ceramic samples.

3.3. Optical and spectroscopic properties

Fig. 6 shows typical Raman spectra of the samples Lu0, Lu11, Lu23 and 1 at.% Yb:Lu_2O_3 ceramic. In the following discussion the Raman peaks considered in the analysis will be arbitrarily designated as R1, R2, R3 (see Fig 6). Their positions were found in good agreement with literature data [[27]] for the two end compositions (*i.e.* Y_2O_3 and Lu_2O_3). The main Raman modes of Y_2O_3 are located at 379, 471 and 595 cm^{-1} whereas the corresponding Raman modes of Lu_2O_3 are located at 393, 499 and 610 cm^{-1}. The system has then adequate resolution to discriminate the Raman peaks

of Y_2O_3 from those of Lu_2O_3. In the mixed compositions, these Raman modes show an increase in their shift which is about linear with the concentration of Lu as shown in Fig. 7.

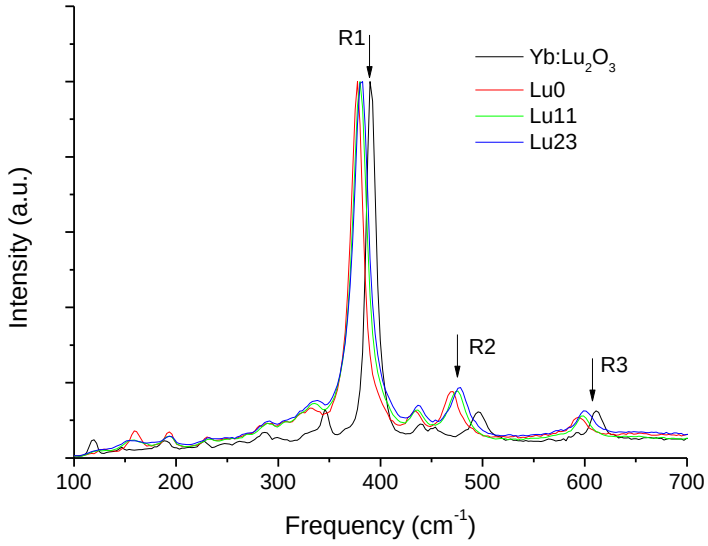

Fig. 6. Raman spectra of the samples under tests. The Raman modes considered in the analysis have been arbitrarily labeled as R1, R2 and R3.

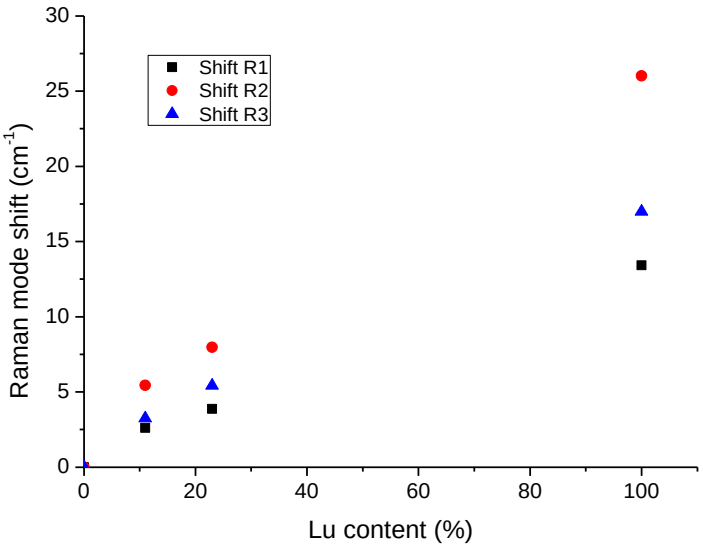

Fig. 7. Peaks shifts in the Raman spectra for increasing Lu content.

The spatial resolution of the instrument is about 1 µm in horizontal (*i.e.* across the line of sight) as well as in vertical (*i.e.* along the line of sight) direction: vertical resolution is provided by the confocal arrangement of the optical set-up. The probed volume is therefore smaller than the average grain size, see Fig. 4. The micro-Raman characterization has shown that the composition of the samples is spatially homogeneous, without reciprocal segregation or separation between Lu_2O_3

and Y_2O_3. In other words, Lu^{3+} and Y^{3+} ions are well mixed in the samples, at least at the 1 µm spatial scale. The Raman spectra acquired on different points of the sample with Lu23 did not show appreciable variations from point to point (Fig. 8). The position and the width of the Raman peaks remain the same for all the points in the analyzed transect: this is a strong indication that the composition of the sample is homogeneous in the different points. Variation in the composition, indeed, should appear as a variation in the position of the peaks along the scan or, in case of coexisting Y_2O_3 and Lu_2O_3 phases in the same probed volume, as a splitting of the peaks in two sub-peaks, corresponding to the two different compositions.

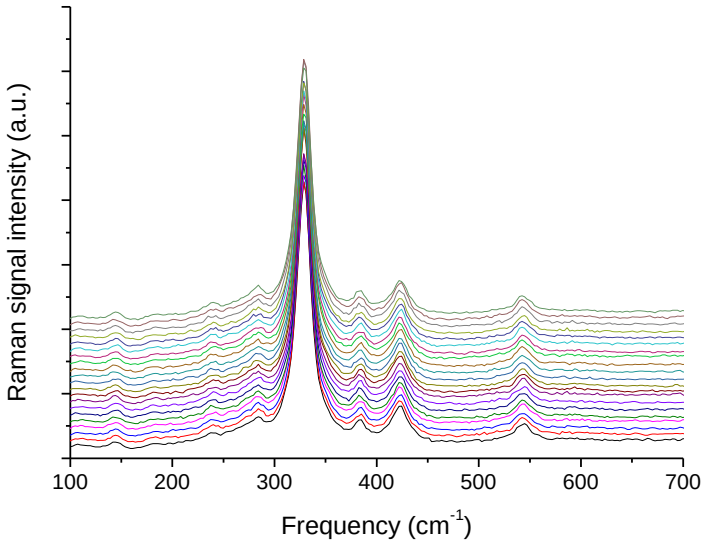

Fig. 8. Raman spectra acquired in 20 different points of the sample Lu23, along a line at steps of 50 µm. Spectra have been shifted vertically for clarity of representation.

A more quantitative information can be gathered by measuring the position of the peaks of the spectra shown in Fig. 8, and using the dependence of the peak position from the Lu/Y fraction, see Fig. 7, to calculate the Lu/Y ratio in the probed volume. For this purpose the lines of the Raman mode R2 (which has the largest sensitivity with respect to the Lu content, *i.e.* 0.37 cm^{-1}/(1*at.%* Lu)) in the individual spectra were fitted by a Gaussian curve, to accurately evaluate the position of the peak. The standard deviation of the peak position for all the spectra acquired along the transect was 0.23 cm^{-1}, corresponding to a standard deviation in the Lu concentration along the transect of 0.085*at.%*. This must be considered as an upper limit in the variation of the concentration of Lu, as this evaluation is of course is also affected by the residual noise in the spectra and not only by the local variation in Lu content.

The transmission spectra reported in Fig. 9 show a very good transparency and very low scattering losses. Even though the theoretical transmission limit cannot be calculated exactly due to

the lack of data for refractive index of $(Lu,Y)_2O_3$, useful insight can be obtained by the evaluation of the transmission for pure Lu_2O_3 and Y_2O_3. The transmission of the samples, far from the Yb^{3+} absorption band, was found very close to the theoretical transmission of the two end compositions.

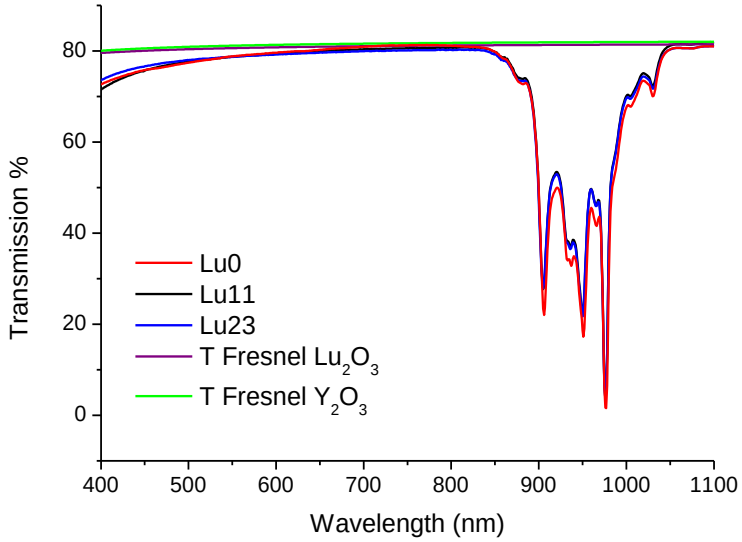

Fig. 9. Transmission spectra of the samples with Lu0 (Yb doping 5.6%, thickness 1.6 mm), Lu11 (Yb doping 5.6%, thickness 1.4 mm) and Lu23 (Yb doping 5.9%, thickness 1.4 mm). Theoretical transmissions of pure Lu_2O_3 and Y_2O_3 (refractive index data by Zelmon *et al.* [[28]]), are also reported.

From the transmission data it is possible to calculate the absorption cross section spectra of the Yb^{3+} lasing transition. The cation site density for the compositions with different Y/Lu balance was calculated by means of the lattice constant data derived from XRD reported in Section 3.2. The resulting spectra are shown in Fig. 10. It can be seen that the increase in the content of Lu^{3+} determines a small shift toward shorter wavelengths of the main absorption peaks at 906 nm and 950 nm as well as of the zero phonon line, of about 0.25 nm for Lu content increasing from 0 to 23.2 mol.%.

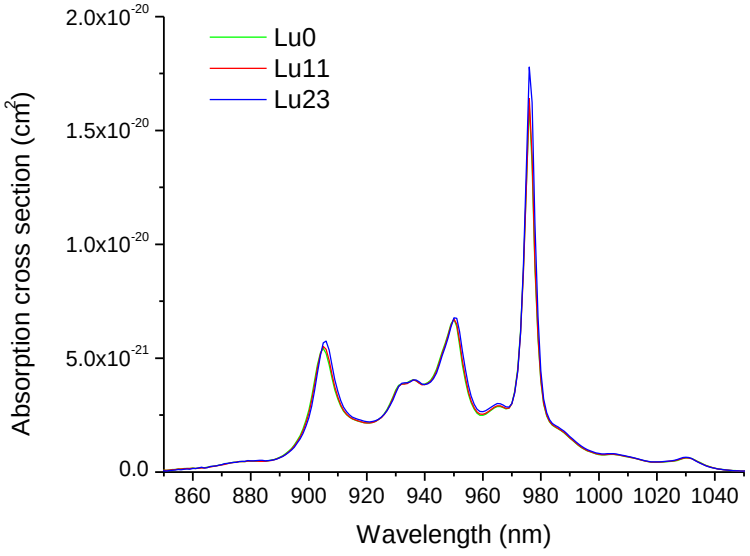

Fig. 10. Absorption cross section spectra for the compositions with different Lu/Y balance.

The fluorescence decay traces from the three samples under test, acquired with a 300 µm pinhole diameter, are shown in Fig. 11. The calculated lifetimes are reported in Table 2, along with literature data for the two end-composition, Yb:Lu_2O_3 and Yb:Y_2O_3. A decreasing value of the upper level lifetime for increasing Lu content, *i.e.* form 782 µsec for Lu0 to 695 µsec for Lu23 is observed. There is some spread in the literature values of the upper level lifetime of Yb in Y_2O_3 and in Lu_2O_3 as well; the value that we measured for Y_2O_3 is near to the upper limit of the literature data [[29]]. On the other hand, for increasing Lu^{3+} concentration the lifetime decreases to a value near to the lower level of literature data, even farther from the value of Yb:Lu_2O_3. Our interpretation is that the samples under test experienced an increase of the non-radiative decay probability for increasing Lu^{3+} content, probably due to an increasing lattice defect density.

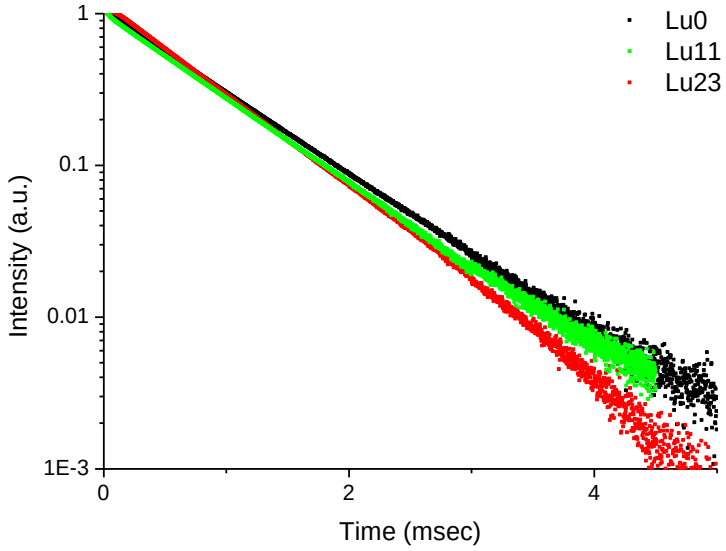

Fig. 11. Decay traces of the luminescence emitted by the samples with different Y/Lu balance, using a pinhole with 300 µm diameter. Intensity is expressed as log scale.

Table 2. Lifetime of the Yb^{3+} upper laser level ($^2F_{5/2}$) for the different tested ceramics compositions . The literature values for the end compositions Yb:Y_2O_3 and Yb:Lu_2O_3 have been also reported.

Composition	Yb^{3+} $^2F_{5/2}$ lifetime	Reference
Lu0	782 µsec	This work
Lu11	757 µsec	This work
Lu23	695 µsec	This work
Yb:Y_2O_3	850 µsec	[[29]]
	720 µsec	[[30]]
	684 µsec	[[31]]
Yb:Lu_2O_3	820 µsec	[[32]]
	805 µsec	[[33]]

The emission cross section spectra were calculated from the fluorescence spectra (see Section 2), using the β-τ method [[34]]. As for the upper level lifetime, whose value is required for the

calculation of the cross section spectrum, we used for all the samples the value of 782 µs found for the sample Lu0; this was considered the best approximation, based on the hypothesis that the values registered with the other compositions are affected by non-radiative decay effects, as discussed above, and they do not correspond to the true radiative lifetime of the upper laser level.

The result of the calculation is shown in Fig. 12. The peak emission cross section is located at about 1030 nm for all the three compositions under test, with a peak value of $1.1\times10^{-20}cm^2$, similar to the value reported for Yb:Y_2O_3 and Yb:Lu_2O_3 in [[11]]. The various compositions show some differences: in particular, the main emission peak at 1032 nm show a broadening of about 2 nm of its FWHM, and the emission peak located near 1076 nm increases its FWHM of about 3.5 nm respectively for the composition with Lu23 with respect to the composition with Lu0.

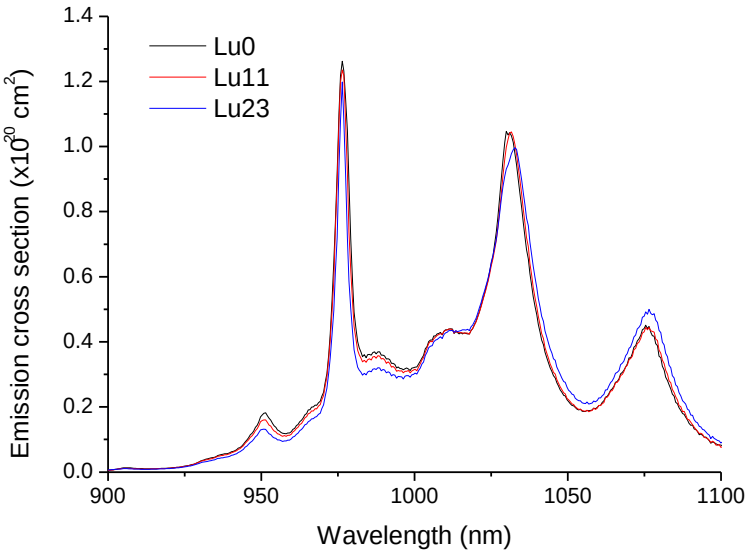

Fig. 12. Emission cross section spectra for the compositions with different Lu/Y balance.

4. Conclusions

In this work we have reported the fabrication, the microstructural properties and the spectroscopic characterization of a new family of Yb doped mixed sesquioxides, namely $(Lu,Y)_2O_3$.

The fabrication method, based on the sintering of laser co-evaporated nanoparticles, has proven very effective to obtain high quality samples, over a broad range of Lu/Y concentration. The transparency of the samples was found very similar to the theoretical limit for the two end compositions, *i.e.* Lu_2O_3 and Y_2O_3. Microstructural characterization was carried out with several different methods, *i.e.* electron microscopy, XRD and micro Raman spectroscopy. XRD evidenced that the samples had the expected cubic crystalline structure, with a decreasing lattice constant for increasing Lu^{3+} content and no secondary phases. Micro-Raman spectroscopy has confirmed that the chemical and structural composition of the ceramics is homogeneous up to the sub-grain size scale, with very small fluctuations in the Lu/Y content from point to point. This indicates that the

use of laser ablated nanopowders as starting material allows obtaining a very fine mixing of Lu_2O_3, Yb_2O_3, Y_2O_3 and ZrO_2 in the individual particles as well as in the green body and therefore a uniform composition after sintering. This allows obtaining a disordered structure at the lattice level, which induces an inhomogeneous broadening of the Yb^{3+} energy levels. Even though the laser ablation does not allow a tight control of the final stoichiometry, this is only a small disadvantage in the production of the continuous substitutional solid solutions analyzed here; this is largely counterbalanced by the possibility to obtain powders which are well mixed down to the nanoscale.

We note here that in order to obtain high optical quality samples, the preparation of sesquioxide ceramics (either mixed or stoichiometric) usually requires special powder preparation methods such as coprecipitation [35] in order to get well mixed powders at the nanoscale. In alternative the use of post-sintering phases as Hot Isostatic Pressing (HIP) is very often required to reduce the residual porosity after the sintering, in particular when simple mixing methods as ball milling are used [37-40] and even when nanoscale coprecipitate powders are used [41]. The use of laser ablated nanopowders allows obtaining high quality ceramics from conventional vacuum sintering, without the use of the costly and complex HIP passage.

The spectroscopic characterization has shown that the mixed composition induces some amount of broadening in the Yb emission spectrum, more evident in the emission peak located near 1077 nm. The overall structure of absorption and emission spectra is intermediate between those of Yb:Lu_2O_3 and Yb:Y_2O_3.

The laser emission properties of these samples will be described in a companion paper on this same Journal [42].

Acknowledgments

Investigation of structural, optical and spectroscopic properties was carried out in the frame of the Joint Bilateral Agreement National Research Council (CNR), Italy / Russian Foundation for Basic Research (RFBR), Russia 2018-2020 (RFBR Grant No. 18-53-7815 Ital_t, CNR project SAC.AD002.020.016). Synthesis and characterization of nanopowders and fabrication of transparent ceramic samples was supported in part by RFBR Grant No. 18-03-00649 A.

The Authors acknowledge the collaboration of Mr. Mauro Pucci of INO-CNR for the optical polishing of the samples.

References and links

[1] Paradis C, Modsching N, Wittwer VJ, Deppe B, Kränkel C, Südmeyer T. Generation of 35-fs pulses from a Kerr lens mode-locked Yb:Lu_2O_3 thin-disk laser. Opt. Express 2017;25(13):14918-14925.

[2] Hornung M, Liebetrau H, Seidel A, Keppler S, Kessler A, Körner J, Hellwing M, Schorcht F, Klöpfel D, Arunachalam AK, Becker GA, Sävert A, Polz J, Hein J, Kaluza MC. The all-diode-pumped laser system POLARIS - an experimentalist's tool generating ultra-high contrast pulses with high energy. High Power Laser Science and Engineering 2014;2:e20.

[3] Luo DW, Xu CW, Zhang J, Qin XP, Yang H, Tan WD, Cong ZH, Tang DY. Diode pumped and mode-locked Yb:GdYAG ceramic lasers. Laser Phys. Lett. 2011;8(10):719-722.

[4] Saikawa J, Sato Y, Taira T, Ikesue A. Absorption, emission spectrum properties, and efficient laser performances of Yb:$Y_3ScAl_4O_{12}$ ceramics. Appl. Phys. Lett. 2004;85(11):1898-1900.

[5] Toci G, Pirri A, Li J, Xie T, Pan Y, Babin V, Beitlerova A, Nikl M, Vannini M. First laser emission of $Yb_{0.15}$:$(Lu_{0.5}Y_{0.5})_3Al_5O_{12}$ ceramics. Opt. Express 2016;24(9):9611-9616.

[6] Tokurakawa M, Kurokawa H, Shirakawa A, Ueda K, Yagi H, Yanagitani T, Kaminskii AA. Continuous-wave and mode-locked lasers on the base of partially disordered crystalline Yb^{3+}:$\{YGd_2\}[Sc_2](Al_2Ga)O_{12}$ ceramics. Opt. Express 2010;18(5):4390-4395.

[7] Wang F, Qin Z, Xie G, Yuan P, Qian L, Xu X, Xu J. 8.5 W mode-locked Yb:$Lu_{1.5}Y_{1.5}Al_5O_{12}$ laser with master oscillator power amplifiers. Appl. Opt. 2014;54(5):1041-1045.

[8] Zhang BT, He JL, Jia ZT, Li YB, Liu SD, Wang ZW, Wang RH, Liu XM, Tao XM. Spectroscopy and laser properties of Yb-doped $Gd_3Al_xGa_{5-x}O_{12}$ crystal. Appl. Phys. Express 2013;6(8):082702-082704.

[9] Lou F, Jia ZT, He JL, Zhao RW, Hou J, Wang ZW, Liu SD, Zhang BT, Dong CM. Efficient High-Peak-Power Wavelength-Switchable Femtosecond Yb:LGGG Laser. IEEE Phot. Technol. Lett. 2015;27(4):407-410.

[10] Lou F, Cui L, Li YB, Hou J, He JL, Jia ZT, Liu JQ, Zhang BT, Yang KJ, Wang ZW, Tao XT. High-efficiency femtosecond Yb:$Gd_3Al_{0.5}Ga_{4.5}O_{12}$ mode-locked laser based on reduced graphene oxide. Opt. Lett. 2013;38(20):4189-4192.

[11] Beil K, Saraceno CJ, Schriber C, Emaury F, Heckl OH, Baer CRE, Golling M, Sudmeyer T, Keller U, Krankel C, Huber G. Yb-doped mixed sesquioxides for ultrashort pulse generation in the thin disk laser setup. Appl. Phys. B 2013;113(1):13-18.

[12] Bagayev SN, Osipov VV, Shitov VA, Pestryakov EV, Kijko VS, Maksimov RN, Lukyashin KE, Orlov AN, Polyakov KV, Petrov VV. Fabrication and optical properties of Y_2O_3-based ceramics with broad emission bandwidth. J. Eur. Cer. Soc. 2012;32(16):4257-4262.

[13] Zhou Z, Guan X, Huang X, Xu B, Xu H, Cai Z, Xu X, Liu P, Li D, Zhang J, Xu J. Tm^{3+}-doped $LuYO_3$ mixed sesquioxide ceramic laser: effective 2.05 μm source operating in continuous-wave and passive Q-switching regimes. Opt. Lett. 2017;42(19):3781-3784.

[14] Li D, Kong L, Xu X, Liu P, Xie G, Zhang J, Xu J. Spectroscopy and mode-locking laser operation of Tm:$LuYO_3$ mixed sesquioxide ceramic. Opt. Express 2019;27(17):24416-24425.

[15] Toci G, Pirri A, Patrizi B, Maksimov RN, Osipov VV, Shitov VA, Yurovskikh AS, Vannini M. High efficiency emission of a laser based on Yb-doped $(Lu,Y)_2O_3$ ceramic. Opt. Mater. 2018;83:182-186.

[16] Kong J, Lu J, Takaichi K, Uematsu T, Ueda K, Tang DY, Shen DY, Yagi H, Yanagitani T, Kaminskii AA. Diode-pumped Yb:Y_2O_3 ceramic laser, Appl. Phys. Lett. 2003;82(16):2556-2558.

[17] Xie GQ, Tang DY, Zhao LM, Qian LJ, Ueda K. High-power self-mode-locked Yb:Y_2O_3 ceramic laser. Opt. Lett. 2007;32(18):2741-2743.

[18] Pirri A, Toci G, Patrizi B, Vannini M. An Overview On Yb-doped Transparent Polycrystalline Sesquioxides Laser Ceramics. IEEE J. Sel. Topics Quantum Electron. 2018;24(5):1602108.
[19] Mun JH, Jouini A, Novoselov A, Yoshikawa A, Kasamoto T, Ohta H, Shibata H, Isshiki M, Waseda Y, Boulon G, Fukuda T. Thermal and Optical Properties of Yb^{3+}-Doped Y_2O_3 Single Crystal Grown by the Micro-Pulling-Down Method. Jap. J. Appl. Phys. 2006;45(7R):5885-5888.
[20] Kong J, Tang DY, Lu J, Ueda K. Spectral characteristics of a Yb-doped Y_2O_3 ceramic laser. Appl. Phys. B 2004;79(4):449-455.
[21] Osipov VV, Platonov VV, Lisenkov VV, Podkin AV, Zakharova EE. Production of nanopowders of oxides by means of fiber and pulse-periodical CO_2 lasers, Phys. Status Solidi C 2013;10(6):926-932.
[22] Osipov VV, Kotov YA, Ivanov MG, Samatov OM, Lisenkov VV, Platonov VV, Murzakaev AM, Medvedev AI, Azarkevich EI. Laser synthesis of nanopowders. Las. Phys. 2006;16(1):116-125.
[23] Richter H, Wang ZP, Ley L. The one phonon Raman spectrum in microcrystalline silicon. Solid. State Comm. 1981;39(5):625-629.
[24] Toci G, Lifetime measurements with the pinhole method in presence of radiation trapping: I-theoretical model. Appl. Phys. B 2012;106(1):63-71.
[25] Toci G, Alderighi D, Pirri A, Vannini M, Lifetime measurements with the pinhole method in presence of radiation trapping: II-application to Yb^{3+} doped ceramics and crystals. Appl. Phys. B 2012;106(1):73-79.
[26] Maksimov RN, Esposito L, Hostasa J, Shitov VA, Belov PA. Densification and phase transition of Yb-doped Lu_2O_3 nanoparticles synthesized by laser ablation. Mater. Lett. 2016;185:396-398.
[27] Laversenne L, Guyot Y, Goutaudier C, Cohen-Adad MT, Boulon G. Optimization of spectroscopic properties of Yb^{3+} doped refractory sesquioxides: cubic Y_2O_3, Lu_2O_3 and monoclinic Gd_2O_3. Opt Mater. 2001;16(4):475-483.
[28] Zelmon DE, Northridge JM, Haynes ND, Perlov D, Petermann K. Temperature-dependent Sellmeier equations for rare-earth sesquioxides. Appl. Opt. 2013;52(16):3824-3828.
[29] Petermann K, Huber G, Fornasiero L, Kuch S, Mix E, Peters V, Basun SA. Rare-earth-doped sesquioxides, J. of Luminesc. 2000;87:973-975.
[30] Boulon G, Laversenne L, Goutaudier C, Guyot Y, Cohen-Adad MT. Radiative and non-radiative energy transfers in Yb^{3+}-doped sesquioxide and garnet laser crystals from a combinatorial approach based on gradient concentration fibers. J. Luminesc. 2003;102-103:417-425.
[31] Auzel F, Baldacchini G, Laversenne L, Boulon G. Radiation trapping and self-quenching analysis in Yb^{3+}, Er^{3+}, and Ho^{3+} doped Y_2O_3, Opt. Mater. 2003;24(1-2):103-109.
[32] Petermann K, Fagundes-Peters D, Johannsen J, Mond M, Peters V, Romero JJ, Kutovoi S, Speiser J, Giesen A. Highly Yb-doped oxides for thin-disc lasers, J. Cryst. Growth 2005;275(1-2):135-140.
[33] Peters R, Krankel C, Petermann K, Huber G. Crystal growth by the heat exchanger method, spectroscopic characterization and laser operation of high-purity Yb:Lu_2O_3, J. Cryst. Growth 2008;310(7-9):1934-1938.
[34] Aull B, Jenssen H, Vibronic interactions in Nd: YAG resulting in non reciprocity of absorption and stimulated emission cross sections, IEEE J. Quantum Electron. 1982;18(5):925-930.
[35] Dai Z, Liu Q, Toci G, Vannini M, Pirri A, Babin V, Nikl M, Wang W, Chen H, Li J. Fabrication and laser oscillation of Yb:Sc2O3 transparent ceramics from co-precipitated nano-powders, J. Eur. Ceram. Soc. 2018(38): 1632-1638.

[36] Wu H., Pan GH, Hao Z, Zhang L, Zhang X, Zhang L, Zhao H, Zhang J. Laser-quality Tm:$(Lu_{0.8}Sc_{0.2})_2O_3$ mixed sesquioxide ceramics shaped by gelcasting of well-dispersed nanopowders, J. Amer. Ceram. Soc. 2019, 102(8): 4919-4928.

[37] Hao Z, Zhang L, Wang Y, Wu H, Pan GH, Wu H, Zhang X, Zhao D, Zhang J. 11 W continuous-wave laser operation at 2.09 μm in Tm:$Lu_{1.6}Sc_{0.4}O_3$ mixed sesquioxide ceramics pumped by a 796 nm laser diode, Opt. Mater. Express 2018 (8): 3615-3621.

[38] Jing W, Loiko P, Serres JM, Wang W, Vilejshikova E, Aguiló M, Díaz F, Griebner U, Huang H, Petrov V, Mateos X. Synthesis, spectroscopy, and efficient laser operation of "mixed" sesquioxide Tm:$(Lu,Sc)_2O_3$ transparent ceramics, Opt. Mater. Express 2017(7):, 4192-4202.

[39] Jing W, Loiko P, Serres JM, Wang Y, Kifle E, Vilejshikova E, Aguiló M, Díaz F, Griebner U, Huang H, Petrov V, Mateos X. Synthesis, spectroscopic characterization and laser operation of Ho^{3+} in "mixed" $(Lu,Sc)_2O_3$ ceramics, J. Lumin. 2018(203): 145-151.

[40] Toci G, Hostaša J, Patrizi B, Biasini V, Pirri A, Piancastelli A, Vannini M. Fabrication and laser performances of Yb: Sc_2O_3 transparent ceramics from different combination of vacuum sintering and hot isostatic pressing conditions. J. Eur. Ceram. Soc. 2020(40): 881-886.

[41] Liu Z, Toci G, Pirri A, Patrizi B, Li J, Hu Z, Wei J, Pan H, Xie T, Vannini M, Li J. Fabrication and laser operation of Yb:Lu_2O_3 transparent ceramics from co-precipitated nano-powders, J. Amer. Ceram. Soc. 2019(102):7491-7499.

[42] Toci G, Pirri A, Patrizi B, Maksimov RN, Osipov VV, Shitov VA, Vannini M. Yb^{3+}:$(Lu_xY_{1-x})_2O_3$ mixed sesquioxide ceramics for laser applications. Part II: Laser performances. Submitted to J. Alloy Compd 2020

Highlights for reviewers

1. First extensive and systematic study of the microstructural and spectroscopic properties of sesquioxide ceramics fabricated with mixed composition $(Lu_x,Y_{(1-x)})_2O_3$ with x=0, 0.113, 0.232 and Yb doping, for laser applications.
2. Application of the laser ablation of the production of well –mixed nanoparticles as starting material for the ceramics.
3. Characterization of the microstructural properties (lattice constant, grain size etc.) for different Lu/Y ratio.
4. Characterization of the internal crystalline phase homogeneity at sub-μm level by means of micro-Raman spectroscopy.
5. Characterization of the spectroscopic properties of Yb^{3+} as optically active dopant for laser applications (absorption and emission cross section spectra, upper laser level lifetimes).

***Declaration of Interest Statement**

Declaration of interests

X The authors declare that they have no known competing financial interests or personal relationships that could have appeared to influence the work reported in this paper.

☐The authors declare the following financial interests/personal relationships which may be considered as potential competing interests:
